ISSN 1063-7729, Astronomy Reports, 2018, Vol. 62, No. 12, pp. 933–939. © Pleiades Publishing, Ltd., 2018.

Structure of the Prompt Emission of GRB 151027A Within the Fireshell Model*♯

D. Primorac[1,2], M. Muccino[1,2], R. Moradi[1,2], Y. Wang[1,2], J. D. Melon Fuksman[1,2], R. Ruffini[1,2], C. L. Bianco[1,2], and J. A. Rueda[1,2]**

[1] *ICRANet, Pescara, Italy*

[2] *ICRA and University of Rome "Sapienza", Physics Department, Rome, Italy*

Received August 1, 2018; in final form, August 25, 2018

Abstract—Long gamma-ray burst GRB 151027A was observed by all three detectors onboard the *Swift* spacecraft, and many more, including MAXI, *Konus*-Wind and *Fermi* GBM/LAT instruments. This revealed a complex structure of the prompt and afterglow emission, consisting of a double-peak gamma-ray prompt with a quiescent period and a HRF/SXF within the X-ray afterglow, together with multiple BB components seen within the time-resolved spectral analysis. These features, within the fireshell model, are interpreted as the manifestation of the same physical process viewed at different angles with respect to the HN ejecta. Here we present the time-resolved and time-integrated spectral analysis used to determine the energy of the e^-e^+ plasma $E_{\rm tot}$ and the baryon load B. These quantities describe the dynamics of the fireshell up to the transparency point. We proceed with the light-curve simulation from which CBM density values and its inhomogeneities are deduced. We also investigate the properties of GRB 140206A, whose prompt emission exhibits a similar structure.

DOI: 10.1134/S1063772918120296

1. INTRODUCTION

Gamma-ray bursts (GRBs) are powerful explosions in distant galaxies, having isotropic equivalent energies $E_{\rm iso}$ ranging from 10^{49}–10^{54} erg. The duration of these transient sources in gamma-rays spans from ms up to a few minutes, with few GRBs lasting up to thousands of seconds (see, e.g., [1, 2]). The burst duration parameter T_{90} is measured as the time interval over which 90% of the total background-subtracted counts are observed, starting when the burst emits 5% of its total measured counts. Bimodality of the T_{90} distribution observed by CGRO/BATSE suggested that different emission mechanisms take place for the two observed distributions. The duration was found to be correlated to the hardness ratio for the entire set of the BATSE data, but not correlated at all for either of the two observed classes of GRBs. Since then, there has been a phenomenological classification of GRBs into long and short ones, with the separation at about 2 seconds [3]. The division was still present if one inquired into their rest frame properties, thanks to the X-ray and optical observations of the GRB afterglows (e.g., see [4]). Today it is generally accepted that the origin of the short GRBs are compact star binary merges [5, 6]. Long GRBs on the other hand are associated with the core-collapse of massive stars. This firm connection is based on the observed spectroscopic supernova (SN) signatures that emerge days later within the optical afterglow light-curve (see, e.g., [7]). GRB localization within their host galaxies further supports this division. Some nearby short GRBs are found in the early-type, low star formation rate galaxies or in the low star formation rate regions of the star-forming galaxies, with a large offset from the host. Long GRBs, on the contrary, are commonly found in the typically irregular galaxies with intense star formation. Thus, long GRBs became traditionally associated with the collapse of a single massive star to a black hole (BH) [8]. Here, the existence of a single ultra-relativistic collimated jet is assumed, where internal or external shocks have a role in the prompt phase emission (the *fireball model*, see, e.g., [9]). However, there are still doubts regarding the central engine (e.g., see [10] for the millisecond magnetar model, and [11] for energetic arguments).

*The article is published in the original.

**E-mail: daracparacldv@hotmail.com

♯Paper presented at the Third Zeldovich meeting, an international conference in honor of Ya.B. Zeldovich held in Minsk, Belarus on April 23–27, 2018. Published by the recommendation of the special editors: S.Ya. Kilin, R. Ruffini, and G.V. Vereshchagin.

Although the existence of the two classes is by now well established, GRB classification based solely on T_{90} may not be sufficient. Firstly, there is a large overlap in the two duration distributions (e.g., [12]). Furthermore, Zhao et al. [13] showed that T_{50} distribution is still bimodal, but with ≈3% of GRBs exchanging classes, where short GRBs are becoming the long ones and vice versa. While for the short GRBs this is due to the boundary effect, the long ones mostly have an unsuitably fitted background. These ones also have the hardness ratio closer to the short bursts. Ideally, the GRB classification method should be free from the potential biases introduced by data analysis, detector sensitivity, redshift measurements and many more. Often that is not the case and prompt emission quantites are very sensitive to the instrument's detection threshold [14]. For example, due to the difference in the covered energy range and the sensitivity, long bursts observed by *Fermi* Gamma-ray Burst Monitor (GBM) have a much longer duration when observed with *Swift* Burst Alert Telescope (BAT) [15]. The opposite happens in the case of short GRBs. This can affect the derivation of the isotropic energy. Shahmoradi & Nemiroff [16] found that the ratio of the observed spectral peak energy $E_{\rm p}$ to the T_{90} is the least-biased GRB classification method into two classes. Others find that the ratio of isotropic gamma-ray energy ($E_{\rm iso}$) and the rest-frame peak spectral energy ($E_{\rm p,\,RF}$) is a more suited parameter to distinguish between the Type I and the Type II GRBs, where TypeI/II is a new, physically motivated classification scheme based on origin [17]. Hints of a third peak within the T_{90} distribution were reported in various papers, suggesting a separate, intermediate class of GRBs. Still, finding out that additional parameters added to a nested model result in a better fit does not mean that the improvement is statistically significant (see, e.g., [18]). In addition to this intermediate class, it was proposed that ultra-long GRBs, lasting for hours, may form a distinct population with a blue supergiant as its progenitor (see, e.g., [19]). Also, there is an open question regarding the X-ray afterglow and whether it should, based on its connection to the central engine, be included in the prompt duration and isotropic energy calculation [20]. In that case, the duration distribution of GRBs should be recalculated. Therefore, there is still an ongoing discussion in the scientific community regarding the GRB classification and its central engine.

In this work, we analyze GRB 151027A prompt emission phase within the Induced Gravitational Collapse (IGC) paradigm. In contrast to the standard fireball/collapsar model, the IGC approach takes into account that SNe Ib/c, associated with long GRBs, mostly occur in double systems [21]. It investigates the impact of the SNe remnant and its role in the prompt emission formation. The starting point of the IGC scenario is a binary system composed of a neutron star (NS) and a carbon–oxygen (CO) core undergoing a SN explosion. From here, a well-determined time sequence is implied, with each stage having distinctive observational properties. This approach then also addresses the multiple components often found with the time-resolved analysis of long GRBs.

After the SN explosion, hypercritical accretion onto a NS takes place thanks to a very efficient neutrino emission, which acts as the main energy sink [22]. A thermal emission often observed in the early seconds of some long GRBs [23] is here interpreted as the soft X-ray emission occurring in the photosphere of the convective outflows (see, e.g., [24]). This will trigger the NS to collapse to a BH, if the accretion rate is high enough ($\gtrsim 10^{-2}-10^{-1} M_\odot\ {\rm s}^{-1}$). If the accretion effectiveness is under $10^{-2} M_\odot\ {\rm s}^{-1}$, the NS will only gain mass. The accretion rate is separation/period dependent, where the separation of $a > 10^{11}$ cm is expected to lead to the creation of a massive NS (MNS). GRBs generated in this fashion are expected to differ in properties. A MNS scenario is expected to produce less energetic GRBs ($\lesssim 10^{52}$ erg), so-called X-ray flashes (XRFs) . On the other hand, interactions of more tightly bound systems that result in the BH creation produce more energetic GRBs ($\gtrsim 10^{52}$ erg) [25], having a distinct afterglow decay [26] and a possible high energy GeV emission associated with the BH formation. Although, the detection of the latter should depend on the inclination of the viewing angle [27]. We address this subclass as binary-driven hypernovae (BdHNe).

In the BdHNe case scenario, optically thick e^+e^- plasma of energy $E^{\rm tot}$ is formed (*the fireshell*). It self-accelerates due to the e^+e^- annihilation, similar as in the fireball model [9]. Upon reaching transparency, a second thermal emission (the P-GRB) can be observed with high Lorentz factor of $\Gamma \sim 10^2-10^3$, in contrast to the previous thermal emission which is almost Newtonian. A shell of baryons, now optically thin, collides with the circumburst medium (CBM), giving rise to the ultra-relativistic prompt emission (UPE). However, this is true only for a small cone opening of ≈10°, defined by the remnant morphology [28]. The system is dynamical. Because of its rotation (∼300 s period), viewing angle with respect to the SN remnant changes. Other areas have much higher particle density due to the remnant. This gives rise to the hard (HXF) and soft (SXF) X-ray flares and the associated, final, extended thermal emission (ETE), which analysis confirms the mildly-relativistic

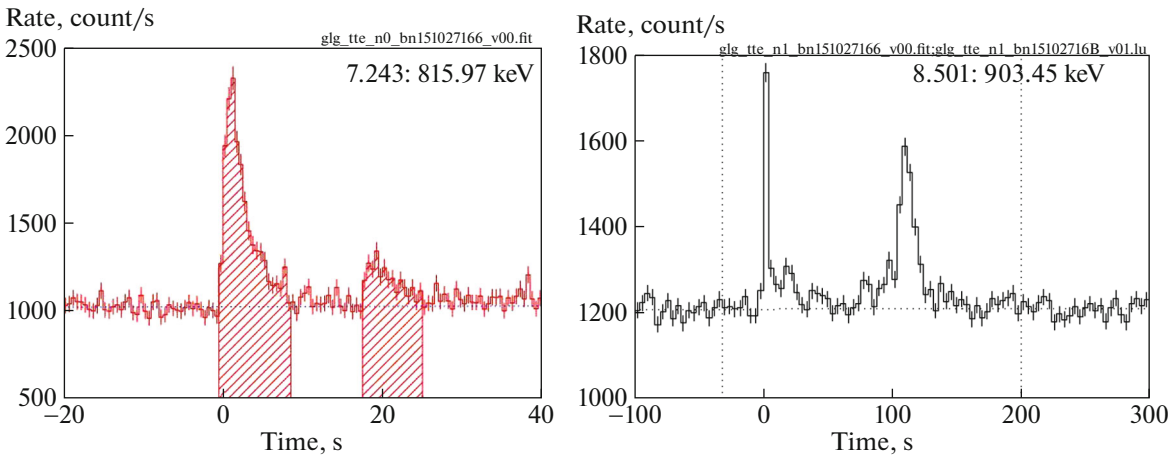

Fig. 1. GRB 151027A GBM-NaI (8–900 keV) light-curve. Two peaks of the UPE phase analyzed in this work are shown on the left, with ≈17 s separation. The entire observed gamma-ray emission is showed on the right, with the HXF starting at 94 s.

regime of this episode. Relativistic treatment shows that the ETE identifies the SN to hypernova (HN) transition. Therefore, these events do not form a causally connected sequence. For more detailed description of each stage, relativistic treatment, numerical simulation results and the comparison between the expected and the obtained properties of such systems, see the recent reviews [25, 29] and references within.

GRB 151027A was detected by multiple observatories and has a vast number of follow-up observations. Thus, it is a good candidate for applying the BdHNe approach, considering the models dependence on the time-resolved and multi-wavelength analysis. As said, here we concentrate on the multiple components in the UPE phase. We perform a P-GRB search through the time-resolved analysis and use simulation of the e^+e^- plasma propagation in order to determine the Lorentz factor and CBM density associated with the UPE. We also investigate the similarities between GRB 151027A and GRB 140206A.

2. TIME-INTEGRATED AND TIME-RESOLVED ANALYSIS OF *FERMI*/GBM DATA

At 3:58:24 UT, the *Swift*/BAT triggered and located GRB 151027A (GCN 18478). The observed light-curve shows two main episodes separated by a quiescent period. The estimated T_{90} in the (15–350 keV) band was 130 seconds. Similar duration, although a bit shorter, was reported by *Konus*-Wind (GCN 18516) and *Fermi*/GBM (GCN 18492). Even though the *Fermi*/LAT (Large Area Telescope) boresight of the source was 10°, there was no detection of high energy photons, suggesting that the line of sight lies in the equatorial plane of the binary system. *Swift* X-ray telescope (XRT) began observing the field 87 s after the trigger, reporting a classiclal FPA light-curve. The first 25 seconds in gamma-rays correspond to the UPE phase in the BdHNe approach. The two peaks, about 8 s in duration (Fig. 1 on the left), are thought to be directly connected to the central engine activity. This activity is again visible later in X-rays, in the form of the HXF (Fig. 1 on the right) and the SXF.

The time-integrated and the time-resolved spectral analysis was performed using the software package RMFIT[1] (version 4.3.2). Both peaks in the UPE phase are best fitted by Compton, as reported by the *Fermi* team, with parameters for the first peak: $E_{\mathrm{p},1} = 172.5(\pm 19.3)$ keV and $\alpha_1 = -1.296(\pm 0.056)$. Second peak parameters are similar, with $E_{\mathrm{p},2} = 147.4(\pm 46.2)$ keV and $\alpha_2 = -1.356(\pm 0.162)$. We calculate isotropic energy using

$$E_{\mathrm{iso}} = \frac{4\pi d_{\mathrm{l}}^2}{(1+z)} S_{\mathrm{bol}}, \qquad (1)$$

where d_{l}^2 is the luminosity distance, $(1+z)$ is the correction factor for the cosmic time dilatation, and S_{bol} is the bolometric fluence in the $1/(1+z)$ keV to $10^4/(1+z)$ keV frame. We determine S_{bol} from a given detection band $(E_{\mathrm{min}}, E_{\mathrm{max}})$ using

$$S_{\mathrm{bol}} = S_{\mathrm{obs}} \frac{\int_{1/(1+z)}^{10^4/(1+z)} E\phi(E)dE}{\int_{E_{\mathrm{min}}}^{E_{\mathrm{max}}} E\phi(E)dE}. \qquad (2)$$

[1] RMFIT for GBM and LAT analysis was developed by the GBM Team and is publicly available at fermi.gsfc.nasa.gov/ssc/data/analysis

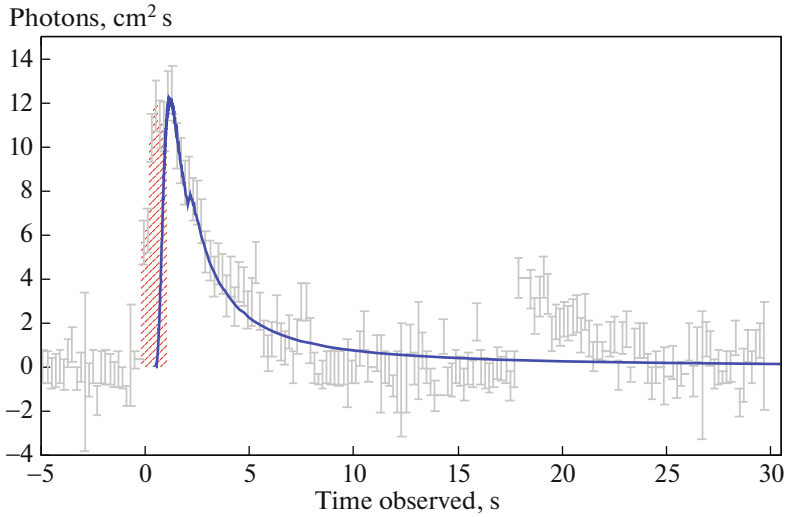

Fig. 2. The observed and the simulated light-curve for the $T_0 + 0.9 - T_0 + 9.44$ s interval of GRB 151027A. The dashed red area marks the P-GRB interval.

Here, ϕ is the Compton model obtained from the spectral fit and $S_{\rm obs} = \Delta t F_{\rm obs}$, where $F_{\rm obs}$ is the mean energy flux during the time interval Δt over which the spectral fit was derived. Considering the reported redshift of $z = 0.81$ (GCN 18487), isotropic energies of the two peaks are: $E_{\rm iso,\,1} = 7.26(\pm 0.36) \times 10^{51}$ and $E_{\rm iso,\,2} = 4.99(\pm 0.60) \times 10^{51}$.

Finally, we perform a time-resolved analysis on the two peaks. While the second peak appears to be featureless, we find an extra black body (BB) component in the first second of the first peak, superimposed on the previous Compton model. This corresponds to the P-GRB emission, when the e^+e^- plasma reaches the transparency point [30]. The best fit model for the $T - 0.1 - T_0 + 0.9$ s time interval was therefore a Compton+BB, with $kT = 36.6(\pm 5.2)$ keV and an energy $E_{\rm BB} = 0.074(\pm 0.038) E_{\rm iso,\,1}$.

3. LIGHT-CURVE AND SPECTRA SIMULATION

Having calculated $E_{\rm iso,\,1}$ and the P-GRB energy, we could proceed to simulate the UPE light-curve and spectra. This is done by solving the equations of the dynamics of the e^+e^- baryon plasma and its interaction with the CBM [31]. By doing this, we can evaluate the ultra-relativistic gamma factor of the UPE at the transparency point and the CBM distribution. Assuming that the initial e^+e^- energy $E^{\rm tot}$ is equal to $E_{\rm iso,\,1}$, for the observed P-GRB temperature we obtain the baryon load $B = 1.92(\pm 0.35) \times 10^{-3}$ and the transparency radius of $r_{\rm tr} = 1.92(\pm 0.17) \times 10^{13}$ cm with Lorenz factor $\Gamma_0 = 503(\pm 76)$. Fitting the UPE light-curve is done by varying the CBM density at different distances. In the IGC paradigm, it is assumed that this emission results from the interaction of the accelerated baryons with the CBM. Agreement with the observed light-curve ($T_0 + 0.9 - T_0 + 9.44$ s, see Fig. 2) and spectra (Fig. 3) was achieved for the average CBM density of $7.46(\pm 1.2)$ cm^{-3}. This is consistent with the typical value of the long GRB host galaxies 10^{16} cm at radii.

4. OBSERVATIONS OF GRB 140206A

Similar to GRB 151027A, GRB 140206A was observed by multiple detectors on various spacecrafts including *INTEGRAL* (GCN 15785), *Swift*/BAT (GCN 15784), and *Fermi*/GBM (GCN 15796). Redshift was reported to be $z = 2.73$ (GCN 15800). Unfortunately, *INTEGRAL* observations encountered technical difficulties. The detection time coincided with the very beginning of the *INTEGRAL* orbit, just outside the radiation belts, making the data polluted by a high particle background. *Fermi*/GBM didn't have more luck. Only the second peak of the GRB has been detected in the GBM data because, during the first peak, the source was occulted by Earth. Therefore, a joined BAT/GBM analysis is needed in the future in order to repeat the procedure as for GRB 151027A. The angle from the *Fermi* LAT boresight was 123 degrees, too far for a meaningful detection of high energy photons.

Nevertheless, BAT observed a multi-peaked structure with a duration of about 90 seconds (Fig. 4). The first pulse duration starts at $\sim T_0 - 15$ and ends at $\sim T_0 + 25$ seconds, and consists of roughly three to four peaks. The second one starts at $\sim T_0 + 50$

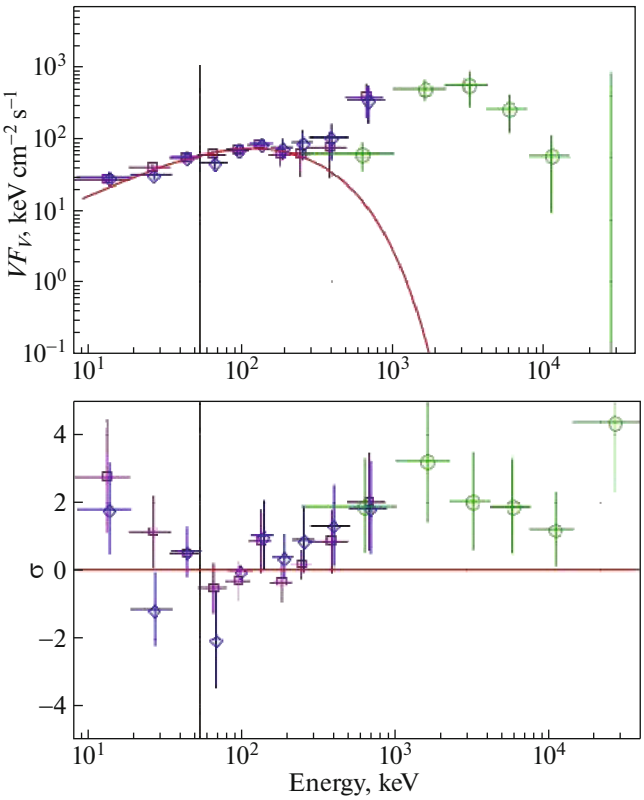

Fig. 3. Simulated spectra of GRB 151027A, superimposed to the observed *Fermi/GBM spectra*. The interval of the time-resolved analysis corresponds to the simulated UPE phase ($T_0 + 0.9 - T_0 + 9.44$ s). There is an agreement between the observed peak spectral energies, where $E_{\rm p,\,obs} = 122.8$ keV and $E_{\rm p,\,sim} = 121.9$ keV.

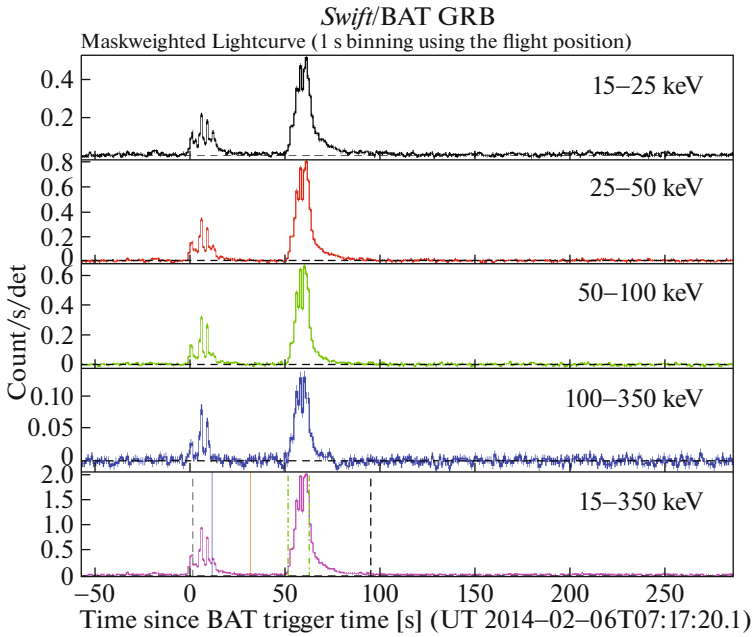

Fig. 4. *Swift*/BAT light-curve in different energy bands of GRB 140206A. Two pulses with the separation of ≈50 s are visible.

and ends at $\sim T_0 + 90$ seconds. There is also a third, weaker pulse peaking at $\sim T_0 + 210$ seconds.

XRT began observations 44 s after the BAT trigger. Light-curve has an initial flaring activity con-

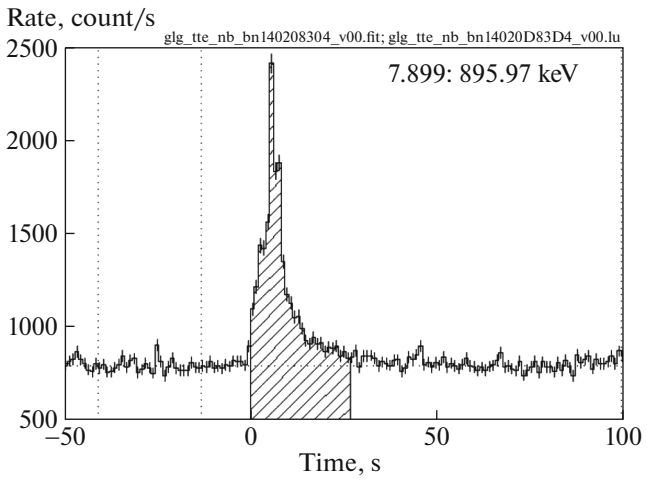

Fig. 5. GBM-NaI light-curve of GRB 140206A. Only second spike is visible. Time interval fitted on different models is showed dashed.

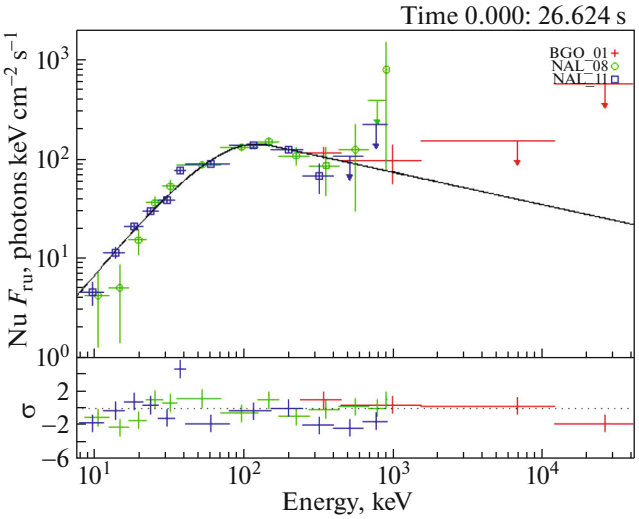

Fig. 6. Best fitted spectral model (Band) for the GRB 140206A T_{90} interval. See the text for parameter values.

sisting of two spikes at about 61 s and 223 s after the trigger. These flares coincide with the second and the third observed gamma-ray spike. This shows that the so-called classical prompt emission and the X-ray afterglow can't always be easily distinguished, and that redefining the duration and E_{iso} parameters should be considered.

A parallel can be drawn between GRB 140206A and GRB 151027A. The first, occulted spike should correspond to the double peak in GRB 151027A, making it an UPE phase of GRB 140206A. The second two peaks, also observed by XRT, should be regarded as the HXF and the SXF within thee BdHNe model. We decided to perform a time-resolved analysis on the second spike using RMFIT package (Fig. 5). We don't find a BB component. Additional analysis of the XRT data should be conducted to investigate the possibility of a thermal signature at lower energies. Band model was the best fitting one (Fig. 6), with $E_p = 123.4(\pm 6.42)$ keV, $\alpha = -0.075(\pm 0.097)$, and $\beta = -2.328(\pm 0.082)$. *Fermi* team reported similar analysis results (GCN 15796).

5. CONCLUSION AND FUTURE WORK

There is still an ongoing discussion regarding the GRB classification and the central engine activity that powers them. In the IGC paradigm, the different observational properties of long GRBs are a direct consequence of the initial binary system separation and the SN ejecta geometry. Based on the NS outcome state, they are divided into the XRF and the BdHNe, where the two are also separated by their energetics and X-ray afterglow light-curves. In this

work we analyzed the GRB 151027A UPE phase and confirmed its ultra-relativistic nature, deriving the CBM density that surrounds the ejecta in the process. The UPE, the HXF, and the SXF are the result of the same physical process of the BH formation and they do not form a casually connected sequence. The time difference between the UPE double component and the flares observed in X-rays is then determined by the propagation of the e^+e^- plasma through the SN ejecta and the rotational period of the system.

ACKNOWLEDGMENTS

This work made use of data supplied by the UK Swift Science Data Center at the University of Leicester.

REFERENCES

1. G. Stratta, B. Gendre, J. L. Atteia, M. Boër, et al., Astrophys. J. **779**, 66 (2013); arXiv: 1306.1699.
2. V. Connaughton, Astrophys. J. **567**, 1028 (2002); astro-ph/0111564.
3. C. Kouveliotou, C. A. Meegan, G. J. Fishman, N. P. Bhat, M. S. Briggs, T. M. Koshut, W. S. Paciesas, and G. N. Pendleton, Astrophys. J. Lett. **413**, L101 (1993).
4. L. Amati, C. Guidorzi, F. Frontera, M. Della Valle, et al., Mon. Not. R. Astron. Soc. **391**, 577 (2008); arXiv: 0805.0377.
5. B. P. Abbott, R. Abbott, T. D. Abbott, F. Acernese, K. Ackley, C. Adams, T. Adams, P. Addesso, R. X. Adhikari, V. B. Adya, et al., Astrophys. J. Lett. **848**, L13 (2017); arXiv: 1710.05834.
6. A. Goldstein, P. Veres, E. Burns, M. S. Briggs, et al., Astrophys. J. Lett. **848**, L14 (2017); arXiv: 1710.05446.
7. M. Della Valle, Int. J. Mod. Phys. D **20**, 1745 (2011).
8. S. E. Woosley, Astrophys. J. **405**, 273 (1993).
9. T. Piran, Phys. Rep. **314**, 575 (1999); astro-ph/9810256.
10. H.-J. Lü and B. Zhang, Astrophys. J. **785**, 74 (2014); arXiv: 1401.1562.
11. A. Maselli, A. Melandri, L. Nava, C. G. Mundell, et al., Science (Washington, DC, U. S.) **343**, 48 (2014); arXiv: 1311.5254.
12. H.-J. Lü, E.-W. Liang, B.-B. Zhang, and B. Zhang, Astrophys. J. **725**, 1965 (2010); arXiv: 1001.0598.
13. X.-H. Zhao, Y.-P. Qin, Y.-M. Dong, and Z.-Y. Peng, Chin. J. Astron. Astrophys. **4**, 349 (2004).
14. N. R. Butler, J. S. Bloom, and D. Poznanski, Astrophys. J. **711**, 495 (2010); arXiv: 0910.3341.
15. F. J. Virgili, Y. Qin, B. Zhang, and E. Liang, Mon. Not. R. Astron. Soc. **424**, 2821 (2012); arXiv: 1112.4363.
16. A. Shahmoradi and R. J. Nemiroff, Mon. Not. R. Astron. Soc. **451**, 126 (2015); arXiv: 1412.5630.
17. B. Zhang, Nature (London, U.K.) **444**, 1010 (2006); astro-ph/0612614.
18. M. Tarnopolski, Astrophys. Space Sci. **361**, 125 (2016); arXiv: 1602.02363.
19. A. J. Levan, N. R. Tanvir, R. L. C. Starling, et al., Astrophys. J. **781**, 13 (2014); arXiv: 1302.2352.
20. G. Ghisellini, G. Ghirlanda, L. Nava, and C. Firmani, Astrophys. J. Lett. **658**, L75 (2007); astro-ph/0701430.
21. N. Smith, W. Li, A. V. Filippenko, and R. Chornock, Mon. Not. R. Astron. Soc. **412**, 1522 (2011); arXiv: 1006.3899.
22. Y. B. Zel'dovich, L. N. Ivanova, and D. K. Nadezhin, Sov. Astron. **16**, 209 (1972).
23. F. Ryde, Astrophys. J. **614**, 827 (2004); astro-ph/0406674.
24. C. L. Fryer, J. A. Rueda, and R. Ruffini, Astrophys. J. Lett. **793**, L36 (2014); arXiv: 1409.1473.
25. R. Ruffini, J. A. Rueda, M. Muccino, Y. Aimuratov, L. M. Becerra, C. L. Bianco, M. Kovacevic, R. Moradi, F. G. Oliveira, G. B. Pisani, et al., Astrophys. J. **832**, 136 (2016); arXiv: 1602.02732.
26. G. B. Pisani, L. Izzo, R. Ruffini, C. L. Bianco, M. Muccino, A. V. Penacchioni, J. A. Rueda, and Y. Wang, Astron. Astrophys. **552**, L5 (2013); arXiv: 1304.1764.
27. R. Ruffini, R. Moradi, Y. Wang, Y. Aimuratov, M. Amiri, L. Becerra, C. L. Bianco, Y.-C. Chen, B. Eslam Panah, G. J. Mathews, et al., arXiv: 1803.05476 (2018).
28. L. Becerra, C. L. Bianco, C. L. Fryer, J. A. Rueda, and R. Ruffini, Astrophys. J. **833**, 107 (2016); arXiv: 1606.02523.
29. R. Ruffini, Y. Wang, Y. Aimuratov, U. Barres de Almeida, et al., Astrophys. J. **852**, 53 (2018); arXiv: 1704.03821.
30. R. Ruffini, Astron. and Astrophys. Suppl. **138**, 513 (1999); astro-ph/9905072.
31. R. Ruffini, J. D. Salmonson, J. R. Wilson, and S.-S. Xue, Astron. Astrophys. **350**, 334 (1999); astro-ph/9907030.